Calibration of ISA accelerometer sensing axes for the BepiColombo mission

Marco Lucente*, Carlo Lefevre, Emiliano Fiorenza, Carmelo Magnafico, Francesco Santoli, Valerio Iafolla

Istituto di Astrofisica e Planetologia Spaziali (IAPS), Istituto Nazionale di Astrofisica (INAF), Via del Fosso del Cavaliere 100 00133, Roma, Italia

Abstract

ISA is a three-axis accelerometer embarked on-board BepiColombo, a joint ESA/JAXA space mission launched on the 19^{th} of October 2018 at 22.45 (local time) and devoted to put two spacecraft (MPO and MMO) around Mercury (2025), for a deeper investigation of the planet and its environment. ISA aims at measuring, directly and not by modelling, first time for a planet other than Earth, the non-gravitational perturbations the MPO will undergo during its stay around Mercury. Such data will be used within the frame of the Radio-Science Experiments to reconstruct, a posteriori and with very high accuracy, the true gravitational orbit of the spacecraft and, at last, the gravity field of Mercury. Three single accelerometers, each one characterised by its own sensing axis, i.e. the direction along which it is sensitive to accelerations, collect the non-gravitational perturbations encountered by the MPO. The arrangement of sensing axes, whose knowledge is essential to reconstruct the sensed accelerations, was measured with very high accuracy by the Experimental Gravitation group at IAPS/INAF in Rome, which manages ISA and holds the PI-ship. The group developed a calibration procedure to identify on-ground the direction of ISA sensing axes with respect to an optical reference frame. An experimental facility was designed and assembled to accomplish the measurement. In November 2015, the calibration was performed on the ISA Flight Model, currently in cruise phase towards Mercury. Results of the measurement campaign are reported and prove the determination of ISA sensing axes with an accuracy within 20-30 arcseconds per single axis, well below the 100 arcseconds required by the Radio-Science needs.

Keywords: accelerometer, ISA, Bepicolombo, Mercury, non-gravitational perturbations, sensor calibration, gravitation

1. Introduction

Mercury is the inner representative of the terrestrial planets class in the Solar System. Very close to the Sun, small and rocky, Mercury has ever represented a challenge among the planets knowledge because of its extreme proximity to the our star. Just two space missions have approached Mercury thus far: Mariner 10, by NASA, collected data during three flybys in 1974-75, whereas MESSENGER (Mercury Surface, Space ENvironment, Geochemistry and Ranging), by NASA as well, concluded in 2015 a four-years stay around the Hermean planet [1].

ESA (European Space Agency) jointly with JAXA (Japan Aerospace Exploration Agency) developed BepiColombo, a cornerstone mission of the Cosmic Vision Programme, with the aim of a deeper and widespread investigation of the planet and of the surrounding environment [2][3]. Named after the Italian scientist Giuseppe "Bepi" Colombo, for his contribution to the study and to the exploration of Mercury, the mission foresees two orbiters, MPO (Mercury Planet Orbiter) and MMO (Mercury Magnetosferic Orbiter), launched on the 19th of October 2018 and currently in cruise phase [4][5], to be placed in complementary polar orbits around Mercury, after about a 6 years-journey and 9 gravity-assists (one at Earth, two at Venus, six at Mercury).

The MPO hosts on-board a suite of advanced scientific instruments (11) to carry

*Marco Lucente
Email address: marco.lucente@inaf.it (Carlo Lefevre, Emiliano Fiorenza, Carmelo Magnafico, Francesco Santoli, Valerio Iafolla)

out several investigations such as imaging, IR-spectroscopy/radiometry, laser altimetry, UV/X-ray/gamma-ray/neutron spectroscopy, radio-science experiments, magnetic field and particle measurements [6][7].

The ISA payload (Italian Spring Accelerometer), a very sensitive three-axial accelerometer, managed by the Experimental Gravitation Group (V. Iafolla PI, F. Santoli PI Deputy) of IAPS (Institute for Astrophysics and Planetology) at INAF (National Institute for Astrophysics) and manufactured by the industrial partner Thales Alenia Space Milan, plays a fundamental role in the Radio-Science Experiments (RSE) [8][9]. The RSEs, carried out by the MORE payload (Mercury Orbiter Radio-science Experiment, [11]) and supported by ISA accelerometer, are a set of intertwined experiments aimed at 1) determining the gravity field of Mercury [12], 2) determining the rotation state of Mercury [13], 3) carrying out some Einstein's General Relativity tests at Mercury and in cruise phase, in order to determine with improved accuracy different parameters, such as the post-Newtonian parameters (γ and β in primis) [18][19][20][21].

The first RSE experiment, also named gravimetry experiment, is designed to provide an accurate estimation of Mercury's gravity field through remarkably stable multi-frequency radio links in X and Ka bands established with the MPO [12][13]. The radio tracking from ground stations at Earth, based on these links, provides high quality range and range-rate measurements to be used for precise orbit determination (POD) and for accurate estimation of the Mercury gravity field. However, the overall spacecraft dynamics, evaluated through those measurements, is ruled by the gravitational field of Mercury (mainly), in addition to the gravity from the Sun and third body effects from other planets, but is affected by Non-Gravitational Perturbations (NGP) as well. The latter ones constitute all the effects on the spacecraft orbit not attributed to gravity. In this frame, pursuing an innovative approach for spacecraft orbiting planets other than Earth, the ISA accelerometer aims at directly sensing the non-gravitational perturbations experienced by the MPO, such as the direct solar radiation pressure and the indirect radiation coming from the planet surface (planetary albedo and infrared emission) [8][9][15]. The direct solar radiation pressure constitutes the leading contribution to NGP over a satellite at the Mercury environment, the solar irradiance being up to 10 times higher than in Earth orbit [15]. Usually, such perturbing effects are evaluated through suitable analytical models. However, results are approximated, since the involved forces are difficult to model: this reduces the accuracy in the orbit determination process [15][16]. In BepiColombo, the direct measurement of NGP through ISA accelerometer is used, at first, to estimate the true gravitational orbit of the MPO, realising (a posteriori) a drag-free spacecraft, and, at last, to determine accurately the Mercury gravity field [12][13]. Finally, the combination of MORE payload and ISA accelerometer foresees the determination of the spherical harmonic coefficients of the Mercury gravity field up to degree and order 25, with a signal-to-noise ratio of 10 [14][13][11].

From a general point of view, the objective of the POD is to define a point on the spacecraft with respect to which to formulate the equation of motion containing the dynamic parameters [17]. Indeed, in a standard orbit determination and parameter estimation procedure, the spacecraft equations of motion are referred to the centre of mass (COM) of the spacecraft. On the other hand, in BepiColombo ISA accelerometer is chosen as reference point to evaluate the overall spacecraft dynamics in the orbit determination process, conversely with respect to the usual approach. This condition allows for simplifying the related equations of motion and to disregard the knowledge of the centre of mass position. In this frame, ISA acts as free-fall test mass in the Mercury gravity field, whose motion is perturbed by external (NGP and gravity gradient) and internal forces (fuel sloshing, solar panel movements, etc.) [9]. Perturbing accelerations are collected through three single accelerometers, arranged to form an orthogonal reference frame within the MPO [22]. Each sensor, constrained to move according to a single degree of freedom, detects accelerations towards a specific direction, defined by its own sensing axis. A sensed acceleration is identified by means of its components towards the ISA sensing axes. To know how the sensing axes are arranged with respect to a suitable reference frame is mandatory, in order to reconstruct correctly the measured perturbing accelerations. The overall accuracy of $10^{-8} m/s^2$, requested by the RSE experiment, is affected by the accuracy in the sensing axes arrangement. At last, measurements collected by sensing axes constitute the output to the RSE experiment.

In this framework, our group at IAPS developed a calibration procedure and an experimental set-up aimed at identifying, on-ground, the direction

of ISA sensing axes with an accuracy within 20-30 arcseconds per axis (at 2σ) with respect to 100 arcseconds required by the RSE experiment. The calibration was carried out in November 2015 on the ISA Flight Model (FM, [24]), currently mounted on MPO spacecraft and on the way to Mercury.

The paper is organised as follows. Section 2 provides a description of ISA accelerometer and its operating principle. Section 3 depicts the calibration procedure of ISA sensing axes and shows the calibration facility developed to measure the sensing axes direction. Section 4 reports the results of the measurement campaign carried out on ISA FM. At last, conclusions are drawn in Section 5.

2. The ISA accelerometer

ISA detects accelerations through three single electro-mechanical accelerometers, assembled to form a three-axis sensor and arranged to constitute an orthogonal reference frame (figure 1) [3][8][22]. Each accelerometer has a sensitivity direction, named sensing axis, i.e. it detects accelerations just towards a specific direction, identified by the normal to the largest surface of the proof mass.[22]. Each ISA sensing element operates as a mono-dimensional damped harmonic oscillator (mass-spring system), forced by an external acceleration (figure 2); an acceleration acting on the frame, induces a displacement of the mass (proof mass). Such a system can be described in the time domain by the well known harmonic oscillator equation of motion. However, a better understanding of the system is achieved in the frequency domain, by applying the Laplace transform to the equation of motion. In this case, the transfer function of the system is obtained, expressing the ratio between the response as mass displacement, Y(s), to the acceleration input X(s):

$$G(s) = \frac{Y(s)}{X(s)} = \frac{1}{s^2 + \frac{\omega_0}{Q}s + \omega_0^2} \quad (1)$$

where ω_0 is the natural angular frequency of the accelerometer ($\omega_0 = 2\pi\nu_0$) and Q its quality factor, related to the dissipation capability. This transfer function, describing a second order dynamical system, returns a flat response for $\omega \ll \omega_0$, where acceleration and displacement are proportional, shows a sharp increase at ω_0 (resonance peak) and decreases fastly for $\omega > \omega_0$ (Figure 3).

In the ISA operating frequency range, the transfer function between the sensed acceleration (a) and the proof mass displacement (x) is flat (within the accuracy required), hence frequency-independent: $x = -a/\omega_0^2$. Hence, the use of very low frequencies allows for increasing the sensor response (x) to detect the very small expected non-gravitational accelerations ($\sim 10^{-7} - 10^{-6} m/s^2$, [15][22]).Indeed, ISA has a very low resonance frequency, $\nu_0 \simeq 3.5\ Hz$ and is made to work in the frequency range $3 \cdot 10^{-5} - 10^{-1} Hz$ with an accuracy up to $10^{-8} m/s^2$ ([8][22]). The mass-spring system previously described is translated into a physical sensor in the figure 4. It shows some elements of a single EQM accelerometer (Engineering Qualification Model, [24]). Each accelerometer, manufactured from a single piece of Al7075, carved through milling machine, is constituted by a sensing element, the proof mass, hanged by a tiny blade to a frame. The blade constitutes the (foil-shaped) spring with a thickness of 140 μm and characterised by a low elastic constant (figure 1).

An acceleration applied to the sensor frame, fixed to the spacecraft, is detected as a displacement of the proof mass, which rotates about the spring rotation axis. The sensed acceleration is measured evaluating the proof mass movement with respect to the frame. Two couples of plates, respectively in the farther and in the closer part with respect to the spring, face the central proof mass to form two capacitors, a capacitive transducer and a capacitive actuator. The first ones, named pick-up plates, are used to gather the sensor response, by detecting any displacement of the proof-mass (figure 4). These plates are included in a capacitance measurement bridge at equilibrium, whereas the other arms consist of known value fixed capacitors. The bridge is biased by a periodic signal coming from a generator and it is decoupled by an isolation transformer. Any sensing mass displacement causes a capacity variation of pick-up plates, hence an unbalancing of the bridge and a modulation of the output voltage [22].

The second couple of capacitors (capacitive actuator) forms the actuators, used to apply electrostatic forces to the proof mass. Their use is envisaged for different reasons: to calibrate the sensor on-flight applying a known acceleration, to set the rest position of the proof mass (operating point), to weaken the torsional spring constant k of the sensor [23]. In particular, the latter action affects the quality factor Q of the sensor, decreasing its value: this allows for tuning the accelerometer sensitivity by using the actuators.

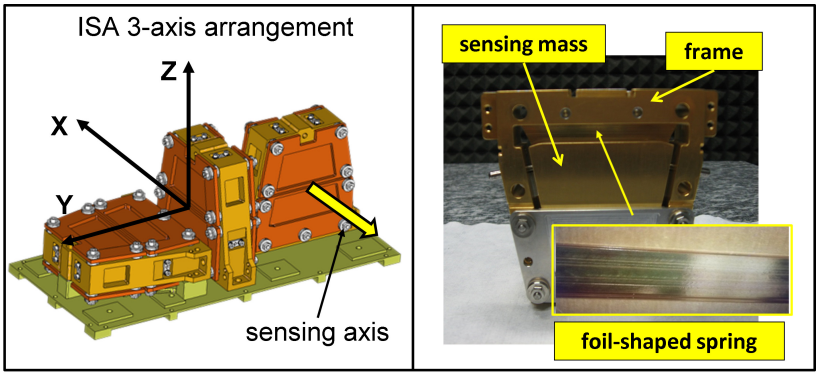

Figure 1: ISA accelerometer arrangement (left, Thales Alenia Space Milan courtesy) and single sensor and related components (right, IAPS)

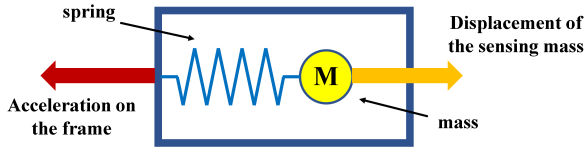

Figure 2: Schematisation of an accelerometer as an harmonic oscillator (mass-spring system)

A 100 μm gap between proof mass and plates is maintained by means of sixteen alumina washers (Al_2O_3), providing electrical insulation as well. Proof mass, plates and washers are assembled by screws and nuts, joining together both sensor sides, preventing the introduction of asymmetry effects.

The frame, joined to the proof mass through the blade, is connected to the electrical ground through a proximity electronics mounted on the frame (not shown here), whose aim is to collect and amplify the signal from plates.

3. The calibration of sensing axes

The ISA on-ground calibration aims at measuring the three sensing axes, i.e. the sensing direction of each accelerometer, defined by the perpendiculars to the proof mass surfaces. The sensed acceleration is straightforwardly reconstructed from its measured projections on the sensing axes. The measurement of the ISA sensing axis direction (SA) is related to the evaluation of the accelerometer response, R, when it rotates with respect to an applied acceleration, $\overrightarrow{A}$. R is the accelerometer output, for instance in terms of voltage signal. Re-

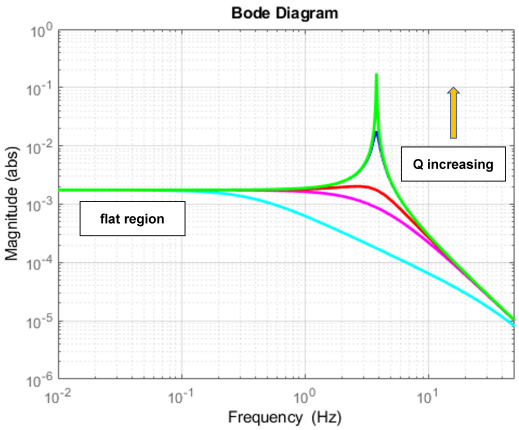

Figure 3: Transfer function for a damped spring-mass system for different values of the quality factor

ferring to figure 5 and, without loss of generality, assuming the acceleration $\overrightarrow{A}$ is in the horizontal plane (XY), the sensor response acts as $R \propto cos\beta$, where β is the angle between $\overrightarrow{A}$ and the sensing axis projection onto XY plane. If $\beta = \pi/2$, i.e. for accelerations perpendicular to the sensing axis, the sensor response would be zero for any direction of application. In this condition, all the accelerations orthogonal to the sensing axis identify a plane, named Non-Sensitivity Plane (NSP). It is worth noticing that as the response $R \propto cos\beta$, its derivative $dR/d\beta \propto -sin\beta$. The response variation, $dR/d\beta$, is almost null around $\beta = 0$, i.e. it undergoes very small variation, whereas is almost one around $\beta = \pi/2$, i.e. it experiences large variation. Consequently, the variation of the accelerometer response is maximised for accelerations normal

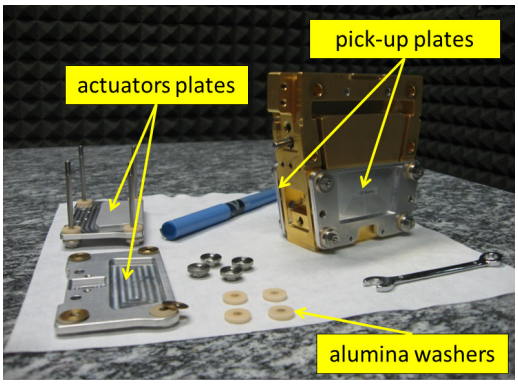

Figure 4: Details of a single ISA accelerometer: pick-up plates (mounted), actuators, screws and washers

to the sensing axis and very reduced for accelerations along the sensing axis. In this condition, an increased resolution in terms of angle is available to identify the sensing axis position. For this reason, the measurement of the sensing axis direction is turned into the identification of the non-sensitivity plane: the sensing axis is straightforwardly the axis perpendicular to this plane.

At last, the most successful strategy for the measurement was to determine indirectly the sensing axis by identifying the non-sensitivity plane. The latter one, defined by the infinite vectors perpendicular to the sensing axis, is obtained through the knowledge of two non-parallel vectors belonging to it, $\overrightarrow{V_1}$ and $\overrightarrow{V_2}$ (figure 6). Once measured these vectors, the sensing axis is derived straightforwardly from the perpendicular to it.

By visualising the NSP as the plane surface of the sensing mass, in order to measure those vectors and due to the sensor geometry, the accelerometer needs to be arranged according to two positions: pendulum and flag configuration (figure 7); the inverse pendulum is not used being not stable under g conditions. These positions allow for putting the sensing axis orthogonal to the acceleration applied and for measuring the two vectors described above. The pendulum configuration was chosen as first one for the calibration. The arrangement of sensing axes needs to be measured with respect to a reference frame, in order to reconstruct correctly the acceleration vector. The UOAF (Unit Optical Alignment Frame), an optical cube fixed to the ISA base, 35-degrees-tilted with respect to it and used as ISA attitude reference with respect to MPO, is suitable to act as reference frame for the measurement (figure 8). The perpendiculars to three faces of the cube with origin into its centre act as UOAF axes. Figure 8 shows the ISA flight model and the UOAF optical cube location.

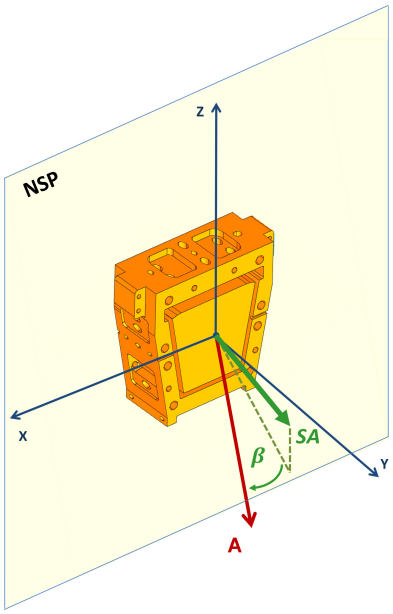

Figure 5: Rotation of the sensor (hence of the sensing axis) by an angle β with respect to an applied acceleration ($\overrightarrow{A}$)

However, from the experimental point of view, a second optical cube, fixed to ISA base and located close to UOAF cube and to ISA corner, is added for different reasons. The first one is the non easy accessibility of the UOAF cube during the calibration procedure. The second one is the need to have accelerometers in dynamics during the measurement and, considering the arrangement in figure 1, the use of a cube with faces parallel to the accelerometer faces helps to put easily in dynamics two of the three sensors. At last, a cube with faces parallel to the sensor faces allows for simplifying the structure of the facility (see figure 13). The reference frame of this second cube, named COC (acronym for calibration optical cube), is identified by the perpendiculars to three faces of the cube, with origin into its centre and UOAF-concordant directions. A rotation matrix, derived measuring the attitude between cubes, is at last applied to bring back the measurement in the UOAF reference.

A calibration facility was designed and assembled to carry out the measurement above depicted. Details are provided in the last subsection of sec-

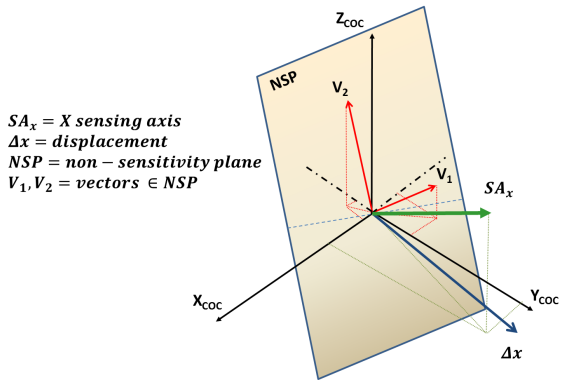

Figure 6: Scheme of the non-sensitivity plane (NSP), identified by ($\overrightarrow{V_1}$) and ($\overrightarrow{V_2}$) , and of the sensing axis (X, as example) with respect to COC frame

tion 3. At last, two phases of measurement need to be accomplished in the framework above outlined. Such phases allow for deriving experimentally two vectors of the NSP for each ISA sensing axis.

3.1. Phase 1

An external excitation, provided by a linear stage through a periodic (sinusoid) displacement with amplitude A and frequency ν, $\Delta x = A \cdot sin(2\pi\nu t + \phi)$, forces ISA to move. The displacement transfers to the proof mass of the measured sensor a corresponding acceleration, whose maximum amplitude is $a = A \cdot (2\pi\nu)^2$. Figure 9 depicts the phase 1 of the measurement. For the sake of clarity, sketches are designed assuming sensor and optical cube fixed, whereas the excitation and the laboratory are able to be rotated around them. Initially, the excitation applied (i.e. the displacement Δx) is arranged towards a direction with respect to the sensing axis (SA_x, assuming X the axis to be measured) and hence to the non-sensitivity plane (figure 9, left). While excited, the sensor is progressively rotated ($\Delta\alpha_1$) until a position is found where the response is null (figure 9, right): α_1 is the corresponding absolute angle, measured by a rotation stage (see later on for the description of the calibration facility). The angle α_1 where the accelerometer returns a (ideally) null response shows that the sensor displacement vector, $\overrightarrow{V_{1x}}$, belongs to the non-sensitivity plane. In this case, ISA moves towards a direction belonging to the non-sensitivity plane of the sensor in measurement. Such a direction identifies a first displacement vector, $\overrightarrow{V_{1x}}$, lying on the NSP. $\overrightarrow{V_{1x}}$ can be evaluated through the measurement of its projections onto the COC frame axes.

A set of three triangulation laser sensors, aimed at the COC faces, was able to measure the projections of $\overrightarrow{V_{1x}}$ onto the COC reference frame. Due to the reflectivity of the cube, the operation of lasers required to tilt the laser beam with respect to the perpendicular to the cube face (through an ad-hoc designed support for lasers). Once the position of nulled sensor response was achieved with the rotation stage, the lasers aimed at three faces of the cube (one laser simed at the face with the perpendicular aligned to the linear stage and two other lasers aimed at the faces orthogonal to it) were put in acquisition to measure the components of $\overrightarrow{V_{1x}}$ in the COC frame. The distance variation measured by lasers was carried out in frequency, by applying an acceleration on the sensor at a certain frequency and recording the peak at that frequency in the spectrum.

3.2. Phase 2

The second phase is a repeat of phase 1 on the same sensor, rotated through 90° around the sensing axis (figure 10, left). In this case, the sensor needs to be arranged in a second configuration, i.e. into flag configuration considering the previous choice. In this position, the excitation Δx is again applied. The accelerometer rotates progressively ($\Delta\alpha_2$) up to find a null response at an angle α_2 (figure 10, right). A second displacement vector, $\overrightarrow{V_{2x}}$, is identified, lying on the NSP. The triplet of lasers aimed at COC cube measures the corresponding $\overrightarrow{V_{2x}}$ components.

3.3. Sensing axis determination

At last, we get two vectors, $\overrightarrow{V_{1x}}$ and $\overrightarrow{V_{2x}}$, belonging to the non-sensitivity plane and not parallel to each other. Assuming the vectors as follows:

$$\overrightarrow{V_{1x}} = [X_1 Y_1 Z_1] \tag{2}$$

$$\overrightarrow{V_{2x}} = [X_2 Y_2 Z_2] \tag{3}$$

the non-sensitivity plane is the plane generated through these vectors, whereas the sensing axis is the vector perpendicular to it. By using just two measurements, the perpendicular could be found straightforwardly through their cross product, as follows:

$$\overrightarrow{SA_x} = \overrightarrow{V_{1x}} \times \overrightarrow{V_{2x}} = \begin{bmatrix} i & j & k \\ X_1 & Y_1 & Z_1 \\ X_2 & Y_2 & Z_2 \end{bmatrix} \tag{4}$$

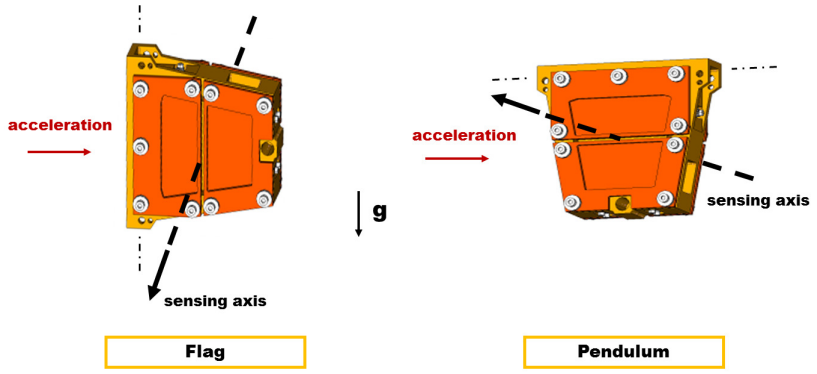

Figure 7: Configurations (flag, pendulum) assumed by the sensor to identify the NSP. The sensing axis is perpendicular to the acceleration applied.

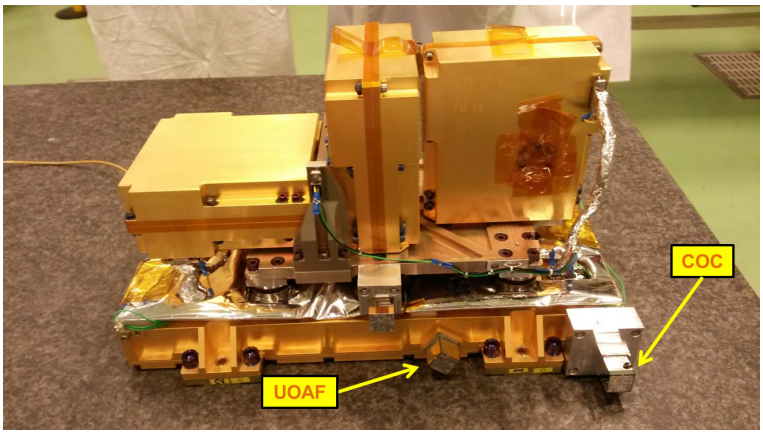

Figure 8: ISA flight model along with UOAF and COC reference systems

However, the collection of repeated measurements of $\overrightarrow{V_{1x}}$, $\overrightarrow{V_{2x}}$ (i.e. $\overrightarrow{V_{1x_i}}$, $\overrightarrow{V_{2x_i}}$, with $i = 1, 2, ...N$) allows for following a different and more rigorous approach, as fully detailed in the data analysis reported in section 4. Actually, the non-sensitivity plane is estimated as the plane which minimises, in the least squares sense, the distances from it of all the measured vectors $\overrightarrow{V_{xi}}$ (both configurations). Finally, the sensing axis is directly obtained as the perpendicular to the plane estimated through the least squares fit.

The search for the orthogonality between the sensing axis to be measured and the applied excitation focuses on the identification of a null response of the accelerometer. However, the response cannot be made null, actually it can be just minimised. The reason is that the sensor does not perform an ideal translation when excited, because of rotations introduced by roll moves of the linear stage. The roll swing, being the sensing axis orthogonal to the excitation during the search for a null response, adds a non-inertial component (gravity), proportional to the roll angle. Such an additional acceleration, being gravity-generated, is not dependent on the frequency of the applied excitation, whereas it depends on $\cos\alpha$, being α the angle between the sensing axis and the perpendicular to the excitation (figure 11). The applied acceleration depends either on $\sin\alpha$ or on the angular frequency ω of excitation. Consequently, the expected output of the accelerometer can be schematised as sum of two contributions, the acceleration due to roll and the acceleration applied, as follows:

$$S_{out} = [(\rho \cdot g) \cdot \cos\alpha - A \cdot \omega^2 \cdot \sin\alpha] \cdot \cos\beta \quad (5)$$

where ρ is the roll angle, ω is the angular frequency of excitation, β is the angle in the vertical plane, A is the displacement amplitude, g the gravitational acceleration. By means of lasers was verified that

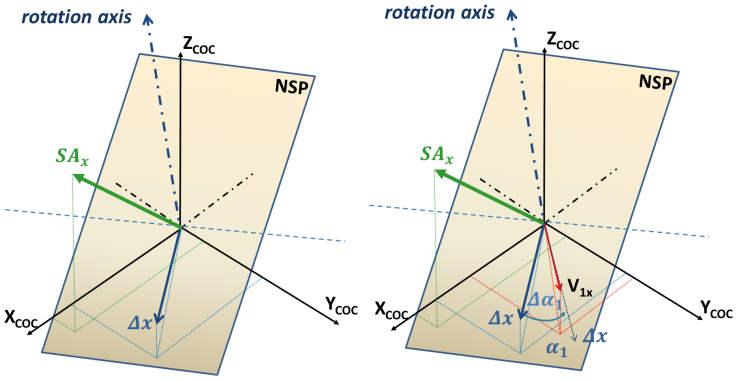

Figure 9: Phase 1: progressive rotation of the sensor up to null the accelerometer response. $\overrightarrow{V_{1x}} \in NSP$.

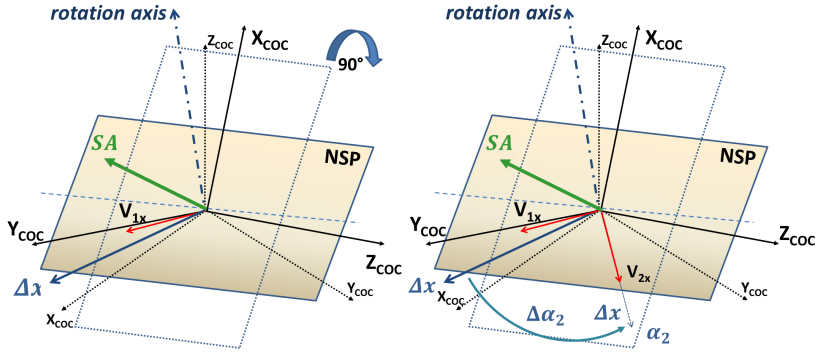

Figure 10: Phase 2: rotation of the sensor through 90° around the sensing axis (left) and progressive rotation of the sensor up to make null the accelerometer response (right). $\overrightarrow{V_{2x}} \in NSP$.

$\beta \simeq 0$, hence the expected output during the measurement is reduced to the following:

$$S_{out} = [(\rho \cdot g) \cdot \cos\alpha - A \cdot \omega^2 \cdot \sin\alpha] \qquad (6)$$

From this equation, the condition $\alpha = 0$, i.e. the sensing axis perpendicular to the excitation, corresponds to find a minimum in the sensor output, $(\rho \cdot g)$. Therefore, the search for the orthogonality position is turned into the search for a minimum response of the sensor. Such a position is experimentally found out through the sampling of the accelerometer output S_{out}, at different angles and angular frequencies. Such outputs are matched with equation 6 through a least squares analysis to find out the best curve fitting data. As example, figure 12 shows the curves obtained during a measurement. Different curves are obtained for different frequencies (equation 6). Curves in the figure interpolate, in the least squares sense, the accelerometer outputs (crosses), measured at different angles (x-axis) and different frequencies (blue = 0.3

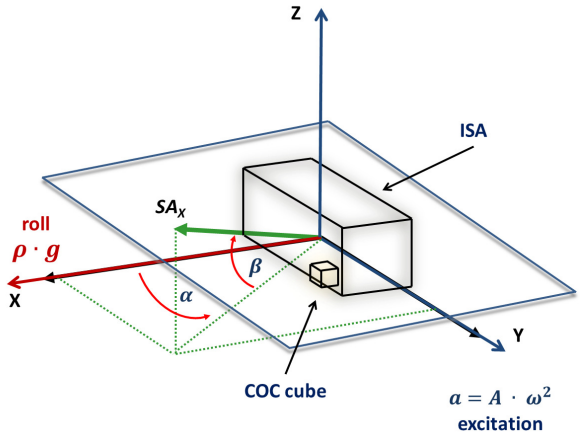

Figure 11: Sketch of the measurement condition when the accelerometer response has to be made null.

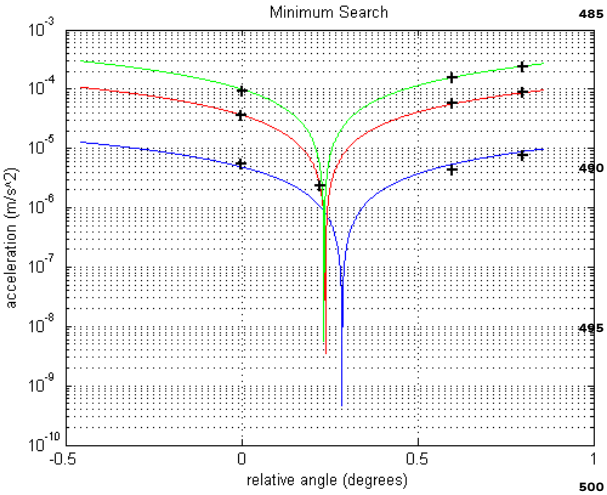

Figure 12: Curves fitting the experimental data at different angles and different excitation frequencies (blue = 0.3 Hz, red = 0.5 Hz, green = 0.6 Hz), according to equation 6

Hz, red = 0.5 Hz, green = 0.6 Hz). The angle α, corresponding to the intersection of curves obtained, identifies the searched minimum response.

3.4. The calibration facility

An experimental set-up was designed and assembled with the aim of executing the calibration procedure. The assembly was made taking into account the different configurations needed to identify the three sensing axes direction: 6 configurations, corresponding to two sensor positions for each axis (pendulum and flag). Main elements of the calibration facility are shown in figure 13. On the top, ISA is fixed within a mechanical interface box, designed to make easier the mounting and the management of the sensor during measurements. On the box sides, three pivots allow for mounting ISA in different positions, depending on the axis in measurement and on the configuration. The COC cube, 15 mm-wide and with faces orthogonal within ± 1 arcsec, is fixed close to a ISA corner. A rotation stage is joined under the mechanical box through an aluminium-made interface and allows for rotating the accelerometer around a vertical axis. It is the Newport RV120HAT, characterised by a range of ± 170 degrees and a resolution of 0.36 arcsec. On the lower part of the rotation stage, a second aluminum-made interface joins a high precision air-bearing linear stage, used to apply accelerations to ISA. It is the Aerotech ABL15005, characterised by a 50 mm run and a roll, pitch and yaw of ± 0.5 arcsec (± $5\mu rad$). The linear stage is fixed to an aluminium-made levelling plane. It is 15 mm-thick and lays on three micrometer screws used to put in dynamics ISA accelerometers. At last, all the assembly leans against a ground-based massive optical bench, providing a very stable, planar and stiff basement with respect to static and dynamical deformations. A couple of orthogonal lasers, through suitable micrometric and positioning stages, is placed (during measurements) close to the COC cube to measure the relative displacements of the sensor. Lasers are triangulation-type produced by the Keyence Japanese company ($\lambda = 650\ nm$, $P = 0.95\ mW$).

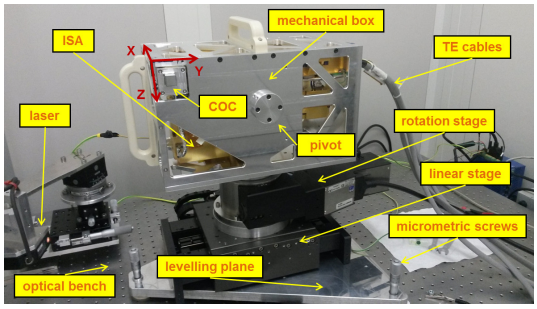

Figure 13: Details of the calibration facility mounted on the optical bench in clean room during the ISA calibration

The calibration facility developed for ISA is a modular assembly with the capability of being adapted and customised, depending on the needs, for the calibration of other electro-mechanical accelerometers. Indeed, the same facility has been adapted and used by our group also to carry out the calibration of HAA (High Accuracy Accelerometer), an accelerometer developed by Thales Alenia Space (Milan) for the JUICE mission [25] to Jupiter and the Galilean moons.

4. Measurements and data analysis

The ISA on-ground sensing axes calibration was carried out in November 2015 at IAPS clean room. Figure 14 shows, as example, the configuration for the search of the minimum response for X accelerometer in pendulum configuration. Gathered data are constituted by an ensemble of vectors obtained through multiple repeats (at different times) of the sensor displacement measurement V_i, corresponding either to a pendulum or to a flag configuration. All these vectors are derived with the con-

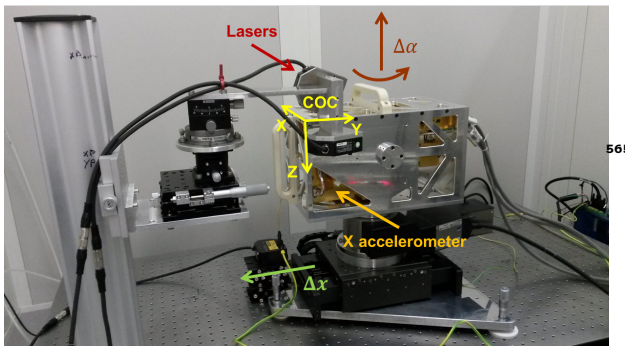

Figure 14: Configuration for the search of the minimum response for X accelerometer at pendulum

straint of being part of the non-sensitivity plane, constraint achieved by imposing the minimisation of the sensor response in each configuration. Moreover, they are almost orthogonal to each other due to the mechanical interface box design and manufacturing. All those vectors would have (ideally) to belong to the same plane, the non-sensitivity plane. Actually, they are spread out around it due to the unavoidable (below a certain threshold) errors, caused by the measurement procedure. However, they can be fitted to find the best plane approximating all the measurements. Hence, the resulting plane would be the plane most likely close to the "true" non-sensitivity plane of the single sensing mass. The best plane fitting the experimental data is derived applying the least squares fit to the measured displacement vectors. Suppose to have N measurements, corresponding to the measured vectors V_i (both configurations) and identified by their components in the COC frame, hence:

$$data = \begin{bmatrix} x_1 & y_1 & z_1 \\ x_2 & y_2 & z_2 \\ x_3 & y_3 & z_3 \\ .... & & \\ x_N & y_N & z_N \end{bmatrix} \tag{7}$$

The goal is to find which is the plane crossing the origin and best fitting the N measured data. Considering the equation of a plane through the origin, as follows:

$$ax + by + cz = d \tag{8}$$

this equation can be written down as explicit form, $z = f(a^{'}, b^{'})$, i.e.

$$z = -a^{'}x - b^{'}y \tag{9}$$

being $a^{'}$ and $b^{'}$ the values to be found out (assimilating c in their values and assuming $c^{'} = 1$). From the point of view of the least squares approach, the problem can be concerned as a two variables linear fit, in which it needs to minimise the following squared sum:

$$z_i - f(a^{'}, b^{'}) = \epsilon_i \tag{10}$$

i.e. we need to change $a^{'}$ and $b^{'}$ up to find the values that minimize ϵ_i^2:

$$min(\sum_{i=1}^{N} \epsilon_i^2) \tag{11}$$

Such a minimisation is equivalent to solve the following linear system:

$$\begin{bmatrix} \sum_{i=1}^{N} x_i^2 & \sum_{i=1}^{N} x_i y_i \\ \sum_{i=1}^{N} x_i y_i & \sum_{i=1}^{N} y_i^2 \end{bmatrix} \begin{bmatrix} a^{'} \\ b^{'} \end{bmatrix} = - \begin{bmatrix} \sum_{i=1}^{N} x_i z_i \\ \sum_{i=1}^{N} y_i z_i \end{bmatrix} \tag{12}$$

where the variables to be found are the parameters $a^{'}$, $b^{'}$, while $c^{'} = 1$. Evaluating the norm, in order to obtain a versor, $n = \sqrt{a'^2 + b'^2 + c'^2}$, we get:

$$a^{"} = \frac{a^{'}}{n} \quad b^{"} = \frac{b^{'}}{n} \quad c^{"} = \frac{c^{'}}{n} \tag{13}$$

therefore, the best fitting mean plane will be the following:

$$a^{"}x + b^{"}y + c^{"}z = 0 \tag{14}$$

where $a^{"}, b^{"}, c^{"}$ are derived through the minimisation. Once identified the plane, the sensing axis is straightforwardly obtained from its coefficients:

$$v = [a^{"}, b^{"}, c^{"}] \tag{15}$$

On the basis of collected measurements it is possible also to evaluate the half-cone standard deviation (at 1σ) of the angular distances as follows:

$$\sigma_{hc} = \sqrt{\frac{1}{N-1} \sum_{i=1}^{N} \theta_i^2} \tag{16}$$

where θ_i is the angular distance of each vector $(x_i,\ y_i,\ z_i)$:

$$\theta_i = \arcsin \frac{D_i}{\sqrt{x_i^2 + y_i^2 + z_i^2}} \tag{17}$$

corresponding to the distance D_i of the same vector from the mean plane and obtained from the following:

$$D_i = a^{'} x + b^{'} y + c^{'} z \tag{18}$$

The mean distance of the vectors from the estimated plane can be evaluated as well through the following:

$$\theta_m = \sum_{i=1}^{N} \frac{\theta_i}{N} \tag{19}$$

By applying the approach depicted above, ISA sensing axes were derived and results are shown in the table 1. It reports the following elements: the components of each axis (considered as versor) in the COC frame ($X_{COC}, Y_{COC}, Z_{COC}$), the half-cone standard deviation (at 2σ) of the angular distances from the non-sensitivity plane (std_{hc}, in arcseconds), the mean distances of measurements from the estimated plane (θ_m, in arcseconds).

In order to figure out the results, angular distances (equation 17) were plotted to show their scattering with respect to the non-sensitivity plane. Figure 15, figure 16 and figure 17 show the relative distribution of such angular distances (rhombus-shaped dots) with respect to the non-sensitivity plane identified by the least mean square method (red line), respectively for X, Y, Z accelerometers. Moreover, the standard deviation σ_{hc} (equation 16) was calculated and a 2σ value was reported in the plot. As shown, all the measures match the estimated non-sensitivity plane assuming a 2σ standard deviation.

X non-sensitivity plane: as shown in figure 15, the experimental measurements are in general distributed very close to the non-sensitivity plane, the most part of them within ±10 arcsec, as few others within ±20 arcsec or less more. However, all the data are in compliance with the non-sensitivity plane (and hence for the corresponding sensing axis) assuming a 2σ standard deviation.

Y non-sensitivity plane: as shown in figure 16, in this case the experimental measurements are spread out very close to the best fitting non-sensitivity plane, the most part of them within ±20 arcsec, just one reaching 30 arcsec. Actually, all the data, apart the latter one, are in compliance with the estimated non-sensitivity plane assuming a 2σ standard deviation. However, the third value (in figure) is in compliance as well, assuming a 3σ standard deviation, i.e. about 37 arcsec. This value is well below

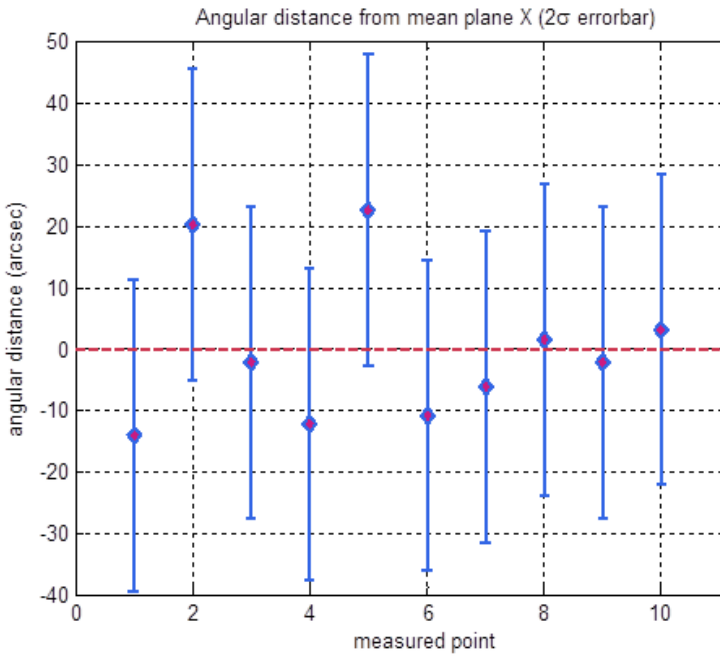

Figure 15: Distribution of measurements evaluated in terms of angular distance from the estimated X non-sensitivity plane. Standard deviation at $2\sigma_0$, $std_{hc} = 25.24$ arcsec

.

the requirement on the sensing axis knowledge (100 arcseconds).

Z non-sensitivity plane: as shown in figure 17, the measurements are distributed within a ±20 arcsec range with respect to the non-sensitivity plane, apart a single value reaching about 30 arcsec. However, all the data are in compliance with the estimated non-sensitivity plane assuming a 2σ standard deviation. On the basis of such data, the angle α_0 between each pair of sensing axes was evaluated as well. Results are shown in table 2. Sensing axes are orthogonal to each other within 0.3 degrees for XY and within 0.03 degrees for XZ and YZ.

5. Conclusions

ISA is a tri-axial accelerometer on-board Bepi-Colombo, a collaborative ESA/JAXA cornerstone space mission which is currently in cruise phase, sending two spacecraft to Mercury planet in 2024. Following an innovative approach for spacecraft orbiting planets other than Earth, ISA aims at measuring, directly and not by modelling, the non-gravitational perturbations affecting the European

Table 1: ISA sensing axes as derived from the least mean square analysis. Details are reported in the text

X Sensing Axis	Components	$2\sigma - std_{hc}$ (arcsec)	θ_m (arcsec)
X_{COC}	$9.9992 \cdot 10^{-1}$		
Y_{COC}	$1.4503 \cdot 10^{-3}$	25.24	-0.051
Z_{COC}	$1.2822 \cdot 10^{-2}$		
Y Sensing Axis	Components	$2\sigma - std_{hc}$ (arcsec)	θ_m (arcsec)
X_{COC}	$-6.7925 \cdot 10^{-3}$		
Y_{COC}	$9.9997 \cdot 10^{-1}$	24.89	-0.342
Z_{COC}	$-1.9907 \cdot 10^{-3}$		
Z Sensing Axis	Components	$2\sigma - std_{hc}$ (arcsec)	θ_m (arcsec)
X_{COC}	$-1.2242 \cdot 10^{-2}$		
Y_{COC}	$2.4100 \cdot 10^{-3}$	29.83	-0.008
Z_{COC}	$9.9992 \cdot 10^{-1}$		

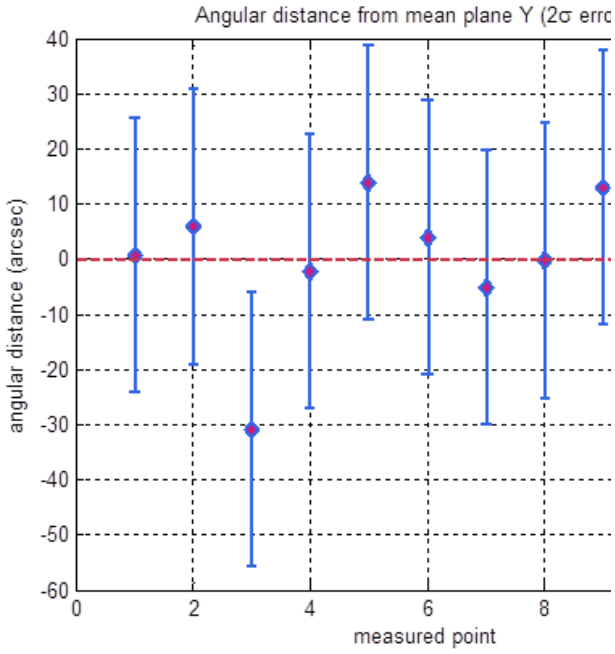

Figure 16: Distribution of measurements evaluated in terms of angular distance from the estimated Y non-sensitivity plane. Standard deviation at $2\sigma_0$, $std_{hc} = 24.89$ arcsec

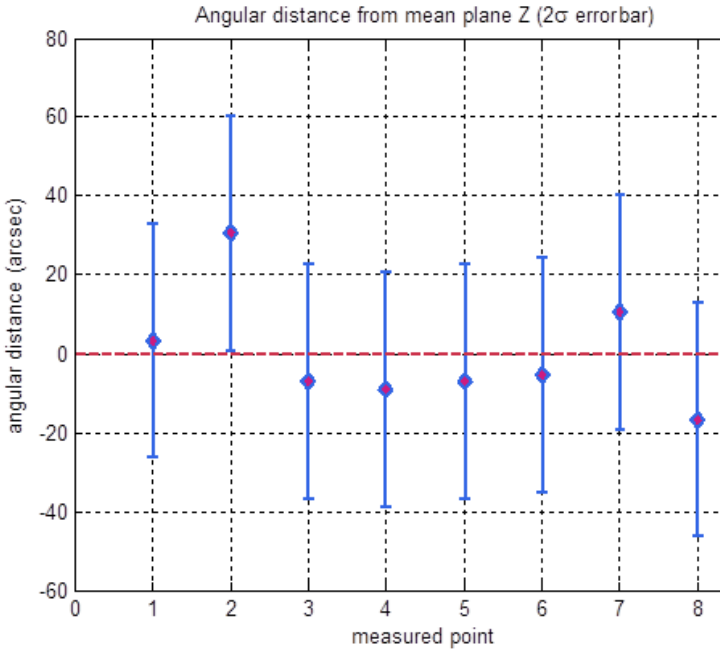

Figure 17: Distribution of measurements evaluated in terms of angular distance from the estimated Z non-sensitivity plane. Standard deviation at $2\sigma_0$, $std_{hc} = 29.83$ arcsec

Table 2: Relative angles between sensing axes

Axes	Angle (degrees)	α_0 (degrees)
XY	89.69	0.31
XZ	89.97	0.03
YZ	90.03	0.03

MPO spacecraft dynamics around Mercury. Such measurements will be used by the Radio-Science Experiment, at first, to estimate the true gravitational orbit of the MPO, making (a posteriori) a drag-free spacecraft, and, at last, to determine accurately the Mercury's gravity field. Each ISA accelerometer detects accelerations towards a particular direction, defined by its own sensing axis. Three single electro-mechanical accelerometers, arranged to form an orthogonal reference frame within the MPO, allow for sensing the perturbing accelerations through the measurement of their components towards the sensing axes. The arrangement of ISA sensing axes, knowledge essential to correctly reconstruct the perturbing accelerations, was measured with very high accuracy by the Experimental Gravitation group at IAPS/INAF in Rome. The team, which manages the ISA accelerometer and holds the PI-ship, developed a calibration procedure aimed at identifying the direction of ISA sensing axes. An experimental set-up was designed and assembled by means of very high performance linear and rotation stages along with triangulation lasers to perform the measurement at IAPS clean room. The calibration procedure was carried out on the ISA Flight Model in November 2015 at IAPS laboratories. Data collected allowed for deriving the direction of sensing axes with respect to an optical cube fixed to ISA and acting as reference frame within the MPO. Reported results showed that sensing axes were obtained with an accuracy within 20-30 arcseconds at 2σ per single axis. Such an accuracy is well within the requested knowledge imposed by the RSE experiment (100 arcseconds per axis).

Acknowledgement

Funding: This research work was performed within the ESA BepiColombo frame, supported by an Italian Space Agency (ASI) contract (No. I/022/10/0). Authors wish to thank Thales Alenia Space Milan, the industrial partner responsible for manufacturing the accelerometer.

References

[1] McNutt R L Jr, Solomon S C, Gold R E, Leary J C and the MESSENGER team 2006 The MESSENGER mission to Mercury: Development history and early mission status *Advances in Space Research* **38** 564-571

[2] Benkhoff J, Casteren J V, Hayakawa H, Fujimoto M, Laakso H, Novara M, Ferri P, Middleton H R and Ziethe R 2010 BepiColombo - Comprehensive exploration of Mercury: Mission overview and science goals *Planetary and Space Science* **58** 2-20

[3] Flamini E, 2011 BepiColombo: the mission, the instruments *Mem. S.A.It.* **82** 386

[4] Santoli, F., Fiorenza, E., Lefevre, C., Lucchesi, D. M., Lucente, M., Magnafico, C., Morbidini, A., Peron, R., Iafolla, V., 2020 ISA, a High Sensitivity Accelerometer in the Interplanetary Space - Updates after the Near-Earth Commissioning Phase of Italian Spring Accelerometer -– ISA *Space Sci Rev* **216** 145

[5] Mangano V.et al., 2021 BepiColombo Science Investigations during Cruise and Flybys at the Earth, Venus and Mercury *Space Sci Rev* **217** 23

[6] Schulz R and Benkhoff J, 2006 BepiColombo: Payload and mission updates *Advances in Space Research* **38** 572-577

[7] Grard R and Balogh A, 2001 Returns to Mercury: science and mission objectives *Planetary and Space Science* **49** 1395-1407

[8] Iafolla V, Fiorenza E, Lefevre C, Morbidini A, Nozzoli S, Peron R, Persichini M, Reale A and Santoli F, 2010 Italian Spring Accelerometer (ISA): a fundamental support to BepiColombo Radio Science Experiments *Planetary and Space Science* **58** 300-308

[9] Iafolla V, Fiorenza E, Lefevre C, Nozzoli S, Peron R, Reale A, Santoli F, 2011 The ISA accelerometer for BepiColombo mission *Mem. S.A.It. Suppl.* **16** 22

[10] Iafolla V, Lucchesi D M, Lucente M, Nozzoli S, Peron R, Santoli F, Argada A, Fiorenza E, Lefevre C, Magnafico C, 2011 The BepiColombo mission to Mercury and the Italian Spring Accelerometer (ISA) role in the Radio Science Experiments measurements *EPSC-DPS Joint Meeting* **6**

[11] Iess L, Asmar S and Tortora P, 2009 MORE: An advanced tracking experiment for the exploration of Mercury with the mission BepiColombo *Acta Astronautica* **65** 666-675

[12] Genova A, Marabucci M and Iess L, 2012 Mercury radio science experiment of the mission BepiColombo *Mem. S.A.It.* **20**, 127

[13] Milani A, Rossi A, Vokrouhlicky D, Villani D and Bonanno C, 2001 Gravity field and rotation state of Mercury from the BepiColombo Radio Science Experiments *Planetary and Space Science* **49** 1579-1596

[14] Cicaló S, Schettino G, Di Ruzza D, Alessi E M, Tommei G and Milani A, 2016 The BepiColombo MORE gravimetry and rotation experiments with the ORBIT14 software *Monthly Notices of the Royal Astronomical Society* **457**, 1507-1521

[15] Lucchesi D M and Iafolla V, 2006 The Non-Gravitational Perturbations impact on the BepiColombo radio Science Experiment and the key role of the ISA accelerometer: direct solar radiation and albedo effects *Celestial Mech Dyn Astr* **96** 99-127

[16] Milani A, Nobili A M and Farinella P, 1987 Non-gravitational Perturbations and Satellite Geodesy

[17] Milani A, Gronchi G, 2010 Theory of Orbit Determination *Cambridge University Press*

[18] Milani A, Vokrouhlicky D, Villani D, Bonanno C and Rossi A, 2002 Testing general relativity with the Bepi-Colombo radio science experiment *Phys. Rev. D* **66** 082001

[19] Imperi L and Iess L, 2015 Testing General Relativity during the cruise phase of the BepiColombo mission to Mercury *2nd IEEE International Workshop on Metrology for Aerospace*, Benevento/Italy, 4-5 June

[20] Milani A, Tommei G, Vokrouhlicky D, Latorre E and Cicaló S, 2009 Relativistic Models for the BepiColombo Radioscience Experiment *Relativity in Fundamental Astronomy: Dynamics, Reference Frames, and Data Analysis, Proceedings*, IAU Symposium No. 261

[21] Will, C M 2006 The Confrontation between General Relativity and Experiment *Living Reviews in Relativity*, [Online Article]: cited /3/2015, http://www.livingreviews.org/lrr-2006-3

[22] Fiorenza E, Lucente M, Lefevre C, Santoli F, Iafolla V, 2016 Zero-g positioning for the BepiColombo ISA accelerometer *Sensors and Actuators A: Physical* **240** 31-40

[23] Pisani M, Astrua M, Iafolla V, Santoli F, Lucchesi D, Lefevre C, Lucente M, 2015 On-ground Actuator Calibration for ISA-BepiColombo *2nd IEEE International Workshop on Metrology for Aerospace*, Benevento/Italy, 4-5 June

[24] ECSS/ESA-Requirements and Standards Division: Space engineering/Verification guidelines ECSS-E-HB-10-02A, from p. 27 (http://escies.org/ftp/ecss.nl/Handbooks/).

[25] Grasset O, Dougherty M K, Coustenis A, Bunce E J, Erd C, Titov D, Blanc M, Coates A, Drossart P, Fletcher L N, Hussmann H, Jaumann R, Krupp N, Lebreton J-P, Prieto-Ballesteros O, Tortora P, Tosi F, Van Hoolst T, 2013 JUpiter ICy moons Explorer (JUICE): An ESA mission to orbit Ganymede and to characterise the Jupiter system *Planetary and Space Science* **78** 1-21